IEEE Access
Multidisciplinary | Rapid Review | Open Access Journal

Received September 19, 2018, accepted October 14, 2018, date of publication October 18, 2018,
date of current version November 14, 2018.

Digital Object Identifier 10.1109/ACCESS.2018.2876647

Aerosol Jet Printed Strain Sensor: Simulation Studies Analyzing the Effect of Dimension and Design on Performance (September 2018)

SHWETA AGARWALA, GUO LIANG GOH, AND WAI YEE YEONG
Singapore Center for 3D printing, School of Mechanical and Aerospace Engineering, Nanyang Technological University, Singapore 639798

Corresponding author: Wai Yee Yeong (wyyeong@ntu.edu.sg)

This work was supported in part by the National Research Foundation (NRF), Prime Minister's Office, Singapore, under its medium-sized center funding scheme for Singapore Centre for 3D Printing and in part by the NTU Startup Grant.

ABSTRACT The 3-D printing has been gaining widespread attention for electronic applications. Aerosol jet printing has emerged as a powerful technique to print new-age sensors and devices on various substrates. In this paper, we use simulation studies to optimize the dimensions and design of aerosol jet printed strain sensor for a good performance. Physical dimensions such as the end loop length, number of grids, grid line width, gauge length, and five different sensor designs are simulated to study their effect on the performance of the strain sensor. This paper helps to identify the factors that affect the sensitivity and gauge factor of the flexible strain sensor fabricated using aerosol jet printing technology.

INDEX TERMS 3D printing, aerosol jet, additive manufacturing, design, performance, simulation, strain sensor.

I. INTRODUCTION

Sensors have been playing an active role in various applications like space shuttle [1], transport [2], aviation [3], and have been incorporate in to new-age electronic devices for measuring quantities like stress, torque, strain, pressure and vibration [4]–[8]. Constant innovation in materials, designs and manufacturing technology has sparked a huge interest in electronic sensors. Nano-sized strain gauges have higher sensitivity and better precision, thus leading to enhanced performance [9], [10]. Conventionally, the fabrication process of a foil strain gauge consists of many steps including bonding, curing, UV-exposing, etching and trimming, thus leading to tedious and inefficient process [11]. Strain gauges have also been fabricated using other methods namely lithographic printing [12], [13], screen printing [14], flexographic printing [15] and inkjet printing [16] on a wide variety of substrates, but most methods are limited in terms of their printing resolution. However, new-age strain gauges have special manufacturing requirements, which sometimes cannot be met using conventional techniques of fabrication. Moreover, traditionally designed strain sensors suffer from limitations like long measurement range, low sensitivity and embedding difficulty in other structures. Hence new ways of fabrication need to be explored. Additive manufacturing (AM) has recently emerged as the key player for fabricating not just three-dimensional (3D) solid objects but novel printed electronic devices such as sensors [17]–[20]. In an AM process, an object is built by laying down layers of material through replicating a computer design file.

Aerosol Jet printing (AJP), a type of additive manufacturing technique, is a non-contact, mask-less method to print electronic inks with fine pitch and high resolution [21]. Aerosol jet printing techniques has many advantages over its counterparts like inkjet and screen printing. AJP can print on 3D surfaces owing to its 5-axis stage; and has higher print resolution. Additive manufacturing for electronics is fairly new, and there is much room to understand how various factors affect the final device parameters and overall performance. Aerosol jet printing has been shown in many works to fabricate various high resolution strain gauge with materials such as silver, carbon nanotubes, PEDOT:PSS on various substrates and structures [22]–[27]. As the technology advances, the sensors need to be smarter, efficient, lighter and robust. This places importance on the design, analysis of stress and measurement of the strain.

Some work has been conducted on simulating MEMS strain gauges and passive wireless strain gauge [28]–[30].

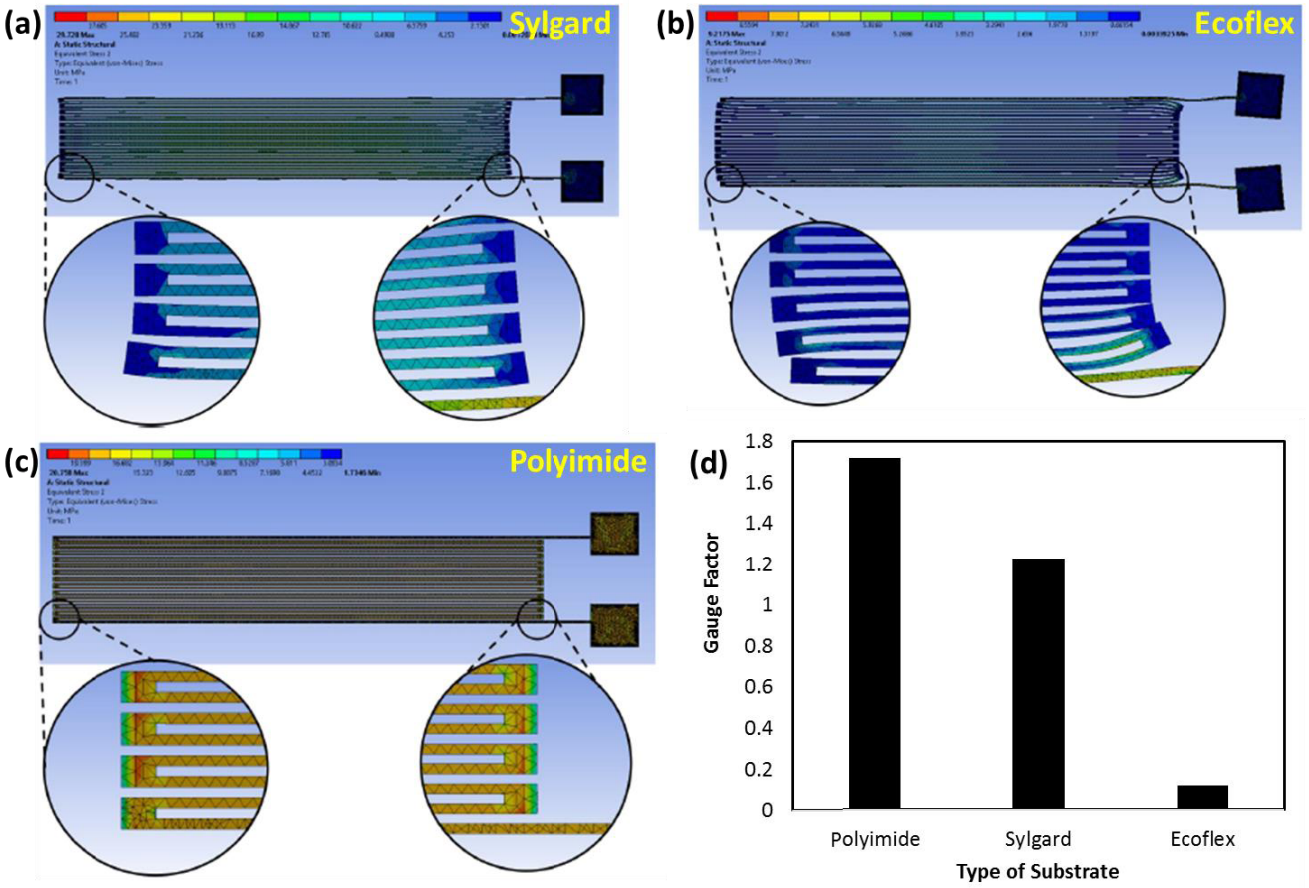

FIGURE 1. Stress analysis on the grid for strain sensor on various substrates namely (a) Sylgard, (b) Ecoflex and (c) Polyimide. (d) Column chart depicting the gauge factor values computed for the strain sensor on different substrates.

However only limited work is available on simulations for thin film piezoresistive strain gauge [31]. This work uses 3D printing technology of aerosol jet to fabricate strain gauge on various substrates. The motivation is to understand the design requirements. Computational simulations are carried out to study the effect of various parameters and design patterns on the overall performance of the fabricated sensor. The study helps to evaluate how different design parameters affect the sensor performance, thus identifying the essential ones for fabricating a sensitive device. The main objective of this project is to use computational simulation to adjust the parameters, design and material of the strain gauge.

II. EXPERIMENTAL SECTION

A. SOFTWARE

SolidWorks modeling software is used to design the strain gauge. For modeling, the grid structure of the strain gauge, substrate and specimen are drawn out individually. Once the modeling is completed, ANSYS Workbench R18.1 version is used to simulate the performance of the strain gauge. In the simulation, static structure and electric analysis are conducted. Static structure is used to simulate the strain gauge when under axial tension load, whereas electric analysis is used to simulate the change in electrical properties when it under axial tension load. For static structure analysis, three meshes of grid structure, substrate and specimen CAD models are created with mesh sizes of 0.000025 m, 0.0001 m, and 0.00077 m respectively. The three meshes are connected together by using bonded contact option in ANSYS. The strain test is done by setting one end of the specimen with fix support and another end with increasing tensile load from 100 N to 1000 N with an interval of 100 N. The simulated result of the static structure analysis is then transferred to the electric analysis for gauge factor calculation. The electrical property of the strain gauge is calculated by passing 1 A current source through the gauge with no voltage at both ends. The resistance change is then calculated by using the simulated potential difference across the gauge. Table 1 shows the materials properties for the substrates, ink and specimens that are used in the simulation.

B. FABRICATION OF STRAIN SENSOR

A working prototype of the strain sensor (grid structure) is fabricated on polyimide substrate using Optomec Aerosol jet 5X system. Kapton® polyimide film with a thickness of 150 μm and dimensions of 50 mm $\times$ 80 mm (width x length) is used as the substrate of choice. Substrate is first cleaned by sonicating in ethanol bath for 10 min. For the

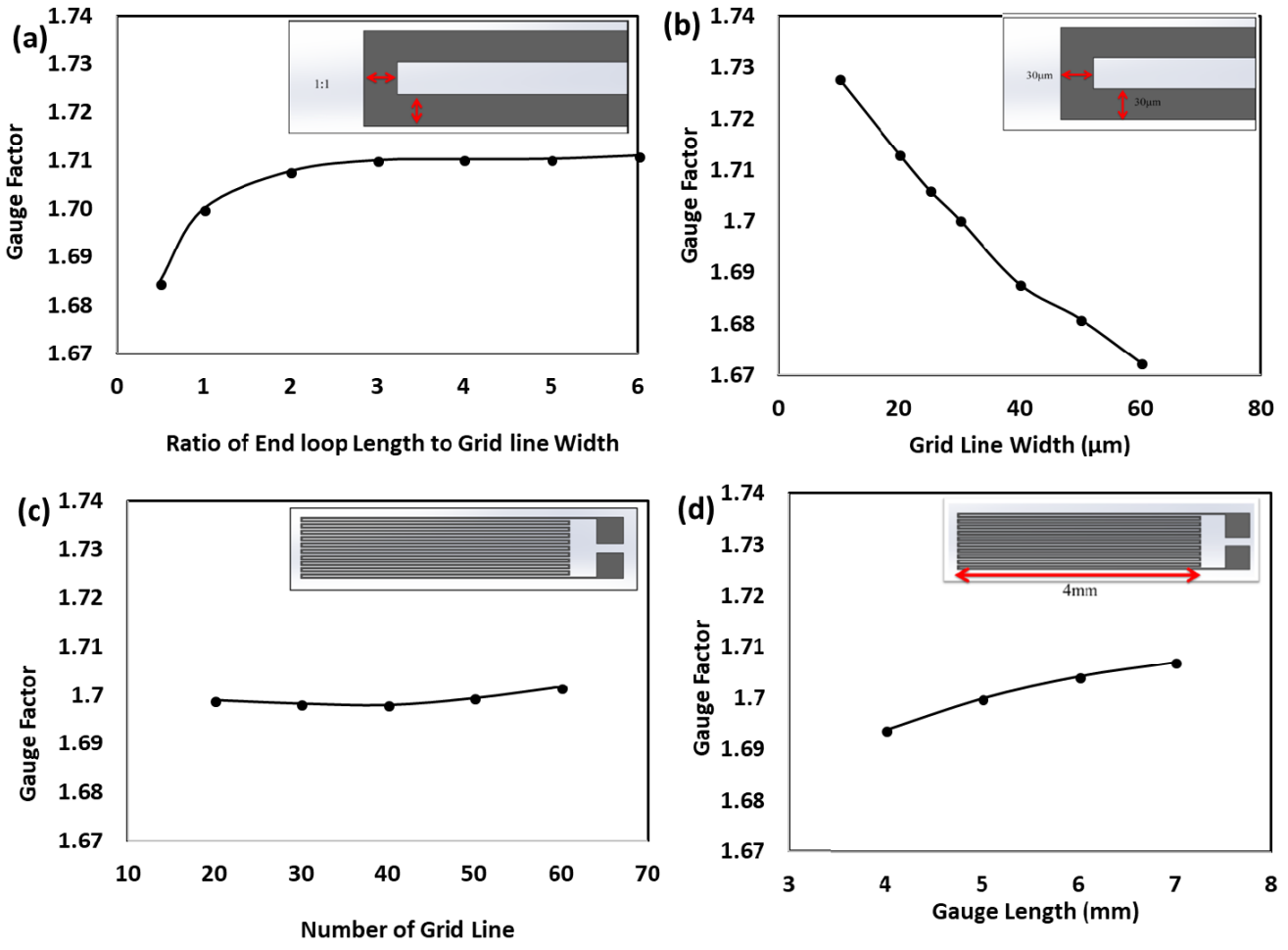

FIGURE 2. Graph depicting the variation in gauge factor with (a) ratio of end loop length to grid line width, (b) grid line width, (c) number of grid lines and (d) gauge length on a strain sensor printed on polyimide substrate.

TABLE 1. Material properties of Ecoflex 00-30, Sylgard 184, Polyimide Film Used in the simulation.

Material properties	Ecoflex 00-30 [A]	Sylgard 184 [A]	Polyimide	Silver [D]	Structural steel [E]
Young's modulus (MPa)	0.66	1.32	2500 [B]	71000	200,000
Poisson's ratio	0.5	0.5	0.35 [C]	0.37	0.3
Resistivity (Ω m)	-	-	-	5.3×10^{-8} [25]	-

[A] Approximated values based on work by Case et al. [32]
[B] Obtained from DUPONT™ KAPTON® Type 100HN Film data sheet.
[C] Obtained from Dolbow et al. [33]
[D] Wilson, J. S. Sensor Technology Handbook Appendix D
[E] Default Material Properties in ANSYS Workbench 18.1

fabrication of the sensor, PRELECT TPS®, Clariant™ silver nanoparticle ink is used. The solid content is 50 wt% in form of silver nanoparticles (size of 30-50 nm). The viscosity and the surface tension of the ink is 10±2 mPa·s. and 35±3 mN/m respectively [34]. The printed sensor pattern is finally sintered at 200 °C for 2 h. Connecting wires are then attached to the sensor by using conductive epoxy. The optimization of printing parameters are similar to our previous work [35]. Aerosol jet printing is carried out using atomizer flow of 30 sccm, Sheath gas flow of 30 sccm, Ultrasonic current of 0.5 A, and process speed of 7 mm/s. A 150 μm nozzle is used and substrate is kept at a temperature of 40 °C. The printed sensors may be attached to the required specimen using quick setting adhesive.

C. CHARACTERIZATION

The printed sensor is strained using a film bending setup. The film bending setup consists of cylinders with known radii (R), varying from 0.5 to 5.0 cm with 0.5 cm increment. The starin gauge printed on a polyimide substrate is pasted on the cylinders using an adhesive such that one of its ends is on the cylinder and the other end is free to move and bend. During the test, the polyimide film is bent on the circumferential side of the cylinders. The strain experienced by the bent polyimide substrate can be calculated using equation (1). Equation 1 is obtained by ignoring the load transfer to the silver film and assuming that the printed silver film is strained at the same

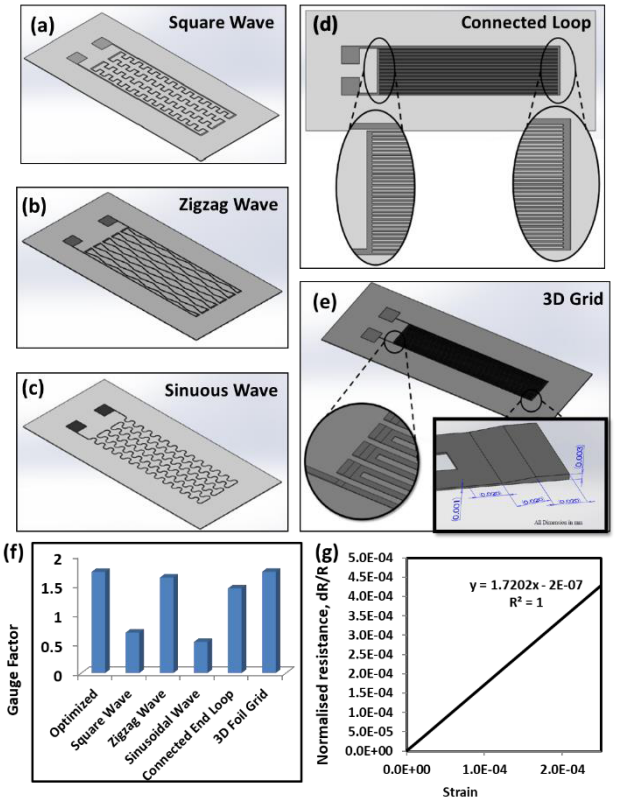

FIGURE 3. Schematic showing different grid designs studied in this work namely (a) Square wave, (b) Zigzag wave, (c) Sinuous wave, (d) Connected end loop and (e) 3D. (f) Chart showing the computed gauge factor values for various grid design. (g) Effect of strain (optimized design) on the electrical property.

rate as the top surface of the polyimide substrate.

$$\frac{\frac{t}{2}}{\frac{t}{2}+R}$$

The change in resistance of the printed sensor is then measured using a digital multimeter (DMM). Connecting wires are attached onto the contact pad of the strain sensor using conductive silver epoxy (cured at 60 °C for 30 min). FESEM images are taken to investigate the line width of the printed strain gauges. 15 measurements are made to ensure statistical meaningful result. The electrical resistance measurement of the strain gauge at each bending radius is repeated five times to ensure accuracy and to obtain statistical meaningful result.

III. RESULTS AND DISCUSSION

Strain gauges use metallic conductors that undergo change in electrical resistance, and this change is recorded as the gauge factor (GF) [36], [37]. Technically, gauge factor can be defined as the ratio of the fractional change in resistance to the fractional change in length (strain) along the axis of the gauge device. Although strain sensor's gauge factor is a crucial factor that determines its performance, there are various other parameters that can affect a sensor's performance. Careful selection of the parameters is important as it affects the performance especially the sensitivity of the sensor.

In this simulation, three different types of substrates are explored namely- Polyimide, Sylgard and Ecoflex. Stress analysis is performed on all the three substrates, which are deformed in the direction of the grid. Figure 1a depicts the stress analysis of the grid on the Sylgard substrate. As can be seen in the magnified image, the grid lines are found to be deformed in the non-linear direction. When the same analysis is performed on Ecoflex substrate, the grid lines are deformed even more (figure 1b). Sylgard and Ecoflex both have the same Poisson's ratio, with Sylgard having a higher Young's modulus. When the substrate is under stress deformation, a stiffer substrate will transfer strain to the grid causing it to deform. On the other hand, a soft and stretchable substrate will resist the transfer of the strain to the grid. The stress analysis on the Polyimide substrate is shown in figure 1c. It can be seen there is not much deformation happens at the edges of the strain sensor. Figure 1d shows the measured GF for all the three substrates. The computed GF of the strain sensor on the polyimide substrate is approximately 1.7202, which is higher than both Sylgard and Ecoflex. Hence, polyimide is the material of choice for fabricating a flexible strain gauge device. It is to be noted that the gauge factor of bulk silver is 4, but the simulated gauge factor is only 1.7202. This can be explained by the non-uniform deformation across the thickness of the substrate and the grid of the gauge. The bottom of the grid (silver) is directly bonded to the top surface of the substrate, while the bottom of the substrate is directly bonded to the top surface of the specimen. Hence both silver and substrate are able to deform freely when the load is applied to the substrate. The compounding effect is that the resultant extension of the grid will be lesser than that of the specimen, which lowers the resistance chance and hence the gauge factor.

Comparing the stress distribution of the foils on different substrates, it is obvious that the stress distribution of the softer materials like Sylgard and Ecoflex is less uniform throughout the grid lines. On a stretchable material, the grid lines at the middle deform less compared to those at the sides of the sensor. As a result, the sensor experiences lesser strain. In other words, stretchable and soft materials cause the sensor to be less effective in detecting the strain as some of the grid lines of the strain sensor are not able to deform as the load is applied. This causes the change in the resistance of the sensor to be lower than expected leading to lower GF. On the other hand, the stress distribution of the grid lines on the polyimide substrate is more uniform, as polyimide material is not stretchable. This results in better stress distribution on the foils and the all the grid lines are able to deform uniformly when load is applied. As a result, the change in resistance of the grid is higher leading to higher GF. The difference in the GF can be attributed to mismatch in Young's modulus of the grid and the substrate materials. A larger mismatch in Young's modulus between the grid and substrate will lead to more resistance in straining compared to the surrounding substrate, thus resulting in non-uniform deformation of

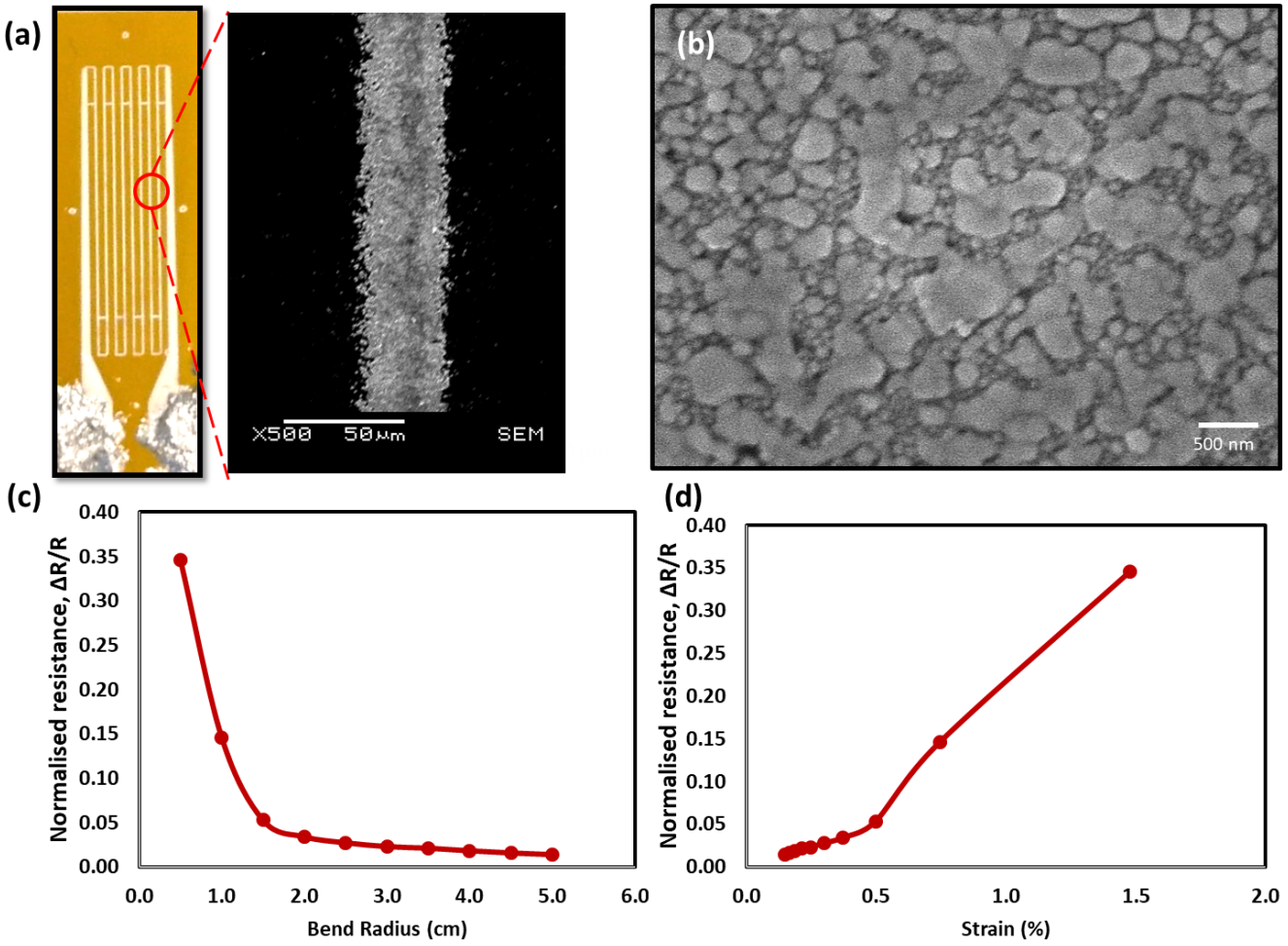

FIGURE 4. (a) Optical image of the aerosol jet printed strain gauge, (b) FESEM image of the silver nanoparticle film after sintering, (c) Change in the normalized resistance with the bending radius and (d) change in normalized resistance with strain on the sensor.

the foil. Conversely, smaller mismatch in Young's modulus will cause the load to be evenly distributed throughout the sensor.

We explore the effect of dimensions in the standard serpentine strain gauge design (as shown in figure 1) and modify the grid design to stimulate its effect on the overall sensor performance through computation modeling. Effect of dimensions is studied first, where the material properties of the substrate, grid and specimen remain unchanged throughout the experiment. Polyimide is used as the substrate of choice, nano-silver as the grid and structural steel for the specimen.

It has been observed that longer end loop length has lower transverse sensitivity and lower creep. However, shortening the end loop length leads to higher fatigue life. The variation in GF of the sensor is stimulated with the ratio of end loop length to grid line width. As can been seen in figure 2a, GF initially increases proportionally and then becomes stable after the ratio reaches value of 3. The trend hints that longer length of the end loop will lead to lower creep of the strain gauge and thus may result in improved performance. Grid line width is another parameter, which can help to improve the sensor performance. A wider grid width is desirable as it helps in better heat dissipation. Sensors with good heat dissipation do not spoil easily during soldering process and tend to have better accuracy as self-heating effect is minimized. Normally the line width has to be carefully decided because if the fabricated sensor has strain gradients perpendicular to the primary axis then narrow grid can help to minimize the error from the effect of shear and Poisson strain. Figure 2b shows the effect of grid line width on the GF. The grid line width is varied from 10 to 60 μm. It can be seen that narrow lines lead to better GF. Apart from the grid line width, number of grid lines are also varied to observe their effect on the GF (figure 2c). Changing the number of grid lines does not significantly affect GF and the sensor performance. It has been reported in literature that more number of grid lines increase the strain resistance, which in turn helps in reducing the heat dissipation. The gauge length is defined as the distance over which the strain is averaged in the sensor device. Gauge length is an important comparison factor between various strain sensors and helps to deduce the behavior of the fabricated device. For this work, the gauge length is varied from 4 to 7 mm. A shorter gauge

length is able to achieve better strain measurement in stress concentrated areas. As can be seen in figure 2d, the shorter gauge lengths lead to smaller GF, thus indicating that there is no stress concentration for the strain sensor used in this work. There is slight increase in the value of GF when the gauge length is increased.

The design of the grid for a strain sensor is equally important to impart required sensitivity and performance. The design of the grid directly affects the sensitivity and gauge factor of the device. This work explores five designs namely square wave, zigzag wave, sinuous wave, connected end loop and 3D grid (figure 3). The material and substrates are same for all the designs. The optimized design of the sensor has dimensions of 3, 60 μm, 20 μm, 5 mm and 26 for ratio of end loop length to grid line width, end loop length, grid line width, gauge length and number of grid lines respectively. 3D grid design is similar to the optimized design of the sensor with the exception that the end loop of the 3D design is thicker as shown in figure 3e, whereas optimized design has uniform thickness throughout the sensor. The line width is 20 μm and the end loop is 60 μm. The thickness of the grid is 1 μm. The detail dimensions of the end loop are shown in figure 3e. It is divided to three different parts based on the thickness. The thickness at the far side of the end loop is 3 μm. It decreases to 1μm to reduce the stress concentrate area. Fig 3f shows the computed gauge factor for each design type along with the optimized standard design. As can be seen, the square and sinuous wave design yield the least gauge factor values of 0.6884 and 0.5282 respectively. This indicates that these two designs make the sensor least sensitive to the strain under tensile force. The zigzag wave design obtained a slightly higher gauge factor. The 3D design obtained the highest gauge factor of 1.7224. However, when compared to the optimized strain gauge design, the gauge factor of 3D grid design is only slightly higher.

The simulation studies are corroborated through experimental results. We fabricated a flexible strain gauge with an average measured line width of approximately 32.13 μm and a standard error of 0.38 μm as shown in figure 4a on polyimide substrate using silver conducting ink. The change in the normalized resistance (normalized with initial strain gauge's resistance) is measured with the bending radius of the strain gauge. The result indicates that the normalized resistance shows a reciprocal trend with bending radius (figure 4c). The result is then replotted in figure 4d for better visualization, thus depicting the effect of the strain due to bending. Interestingly, it is observed that the trend of the normalized resistance of the strain gauge can be categorized into two different regimes, one with a lower GF (strain: 0-0.5%) and other with a higher GF (strain: $>$0.5%) (figure 4d). In the constant GF region, the normalized resistance of the strain gauge varies linearly, and the GF is maintained at values between 9-10. Crack formation may happen at strain values beyond 0.5%, resulting in poor electrical conductivity, thus leading to larger amount of change in the resistance. Since the objective of this paper is to discuss the performance of the strain sensor in its working range (without cracks formation), hence we have limited our simulation study to low strain region, where GF is linear ($<$0.02%). Comparing the GF of the simulated and experimental results, it is observed that the both results show similar linear trends. However, the GF of the experimental result (9-10) is much higher than GF of the simulated result (1.7202). The discrepancy between the experimental and simulated results can be explained by the fact that the simulated result assumes silver film to possess bulk material properties. However silver nanoparticles have properties quite different from their bulk counterparts (figure 4b). It is to be noted that the sensing mechanism of the conducting silver nanoparticle ink does not depend only on the change in the dimensions, but also on the inter-particle spacing, particle size, and homogeneity [38], [39]. The effect of the latter would depend on the choice of materials and heat sintering condition. This explains the limitation and the lower GF value of the simulated result compared to the experimental values. The simulation studies carried out in this paper, help to evaluate various parameters of the strain sensor without the need for physically fabricating them, thus saving time and cost. Different simulation results indicate that the aerosol jet printed strain sensor can be enhanced via computational simulation. The strain sensitivity of the sensor greatly depends on the Poisson's ratio of the grid material, grid dimension and design and the substrate material of the strain gauge.

IV. CONCLUSION

This work is a step forward in the direction of fabricating flexible strain sensor using aerosol jet technology, and trying to select the optimized substrate, foil grid design and dimensions. It was deduced that substrates with high Young's modulus will render more sensitivity to the performance of the sensor. Heightened sensitivity can be achieved when the mechanical properties of the foil grid and substrate are comparable. Different foil grid designs were studied for strain gauge performance. The study further investigated the effect of various dimensions on the strain sensor gauge factor. The optimized parameters were found to be 3 for ratio of end loop length to grid width, 20 μm for the width of the grid lines and 5 mm for the gauge length with 26 grid lines. The parameters obtained using simulation studies were used to fabricate a working model of the sensor using silver conducting ink on polyimide substrate. The optimized strain gauge is measured to have a gauge factor of 9-10 with silver nanoparticle film for the grid.

REFERENCES

[1] P. Hao, D.-Y. Jia, and Z. Yin, "Leak detection and location of seals in spacecraft structures based on a multi-sensor data fusion method," in *Protection of Materials and Structures From the Space Environment*. Beijing, China: Springer, 2017, pp. 563–572.

[2] A. F. de Loza, J. Cieslak, D. Henry, A. Zolghadri, and J. Dàvila, "Sensor fault diagnosis using a non-homogeneous high-order sliding mode observer with application to a transport aircraft," *IET Control Theory Appl.*, vol. 9, no. 4, pp. 598–607, Feb. 2015.

[3] C. A. F. Marques, A. Pospori, D. Sáez-Rodrìguez, K. Nielsen, O. Bang, and D. J. Webb, "Aviation fuel gauging sensor utilizing multiple diaphragm sensors incorporating polymer optical fiber Bragg gratings," *IEEE Sensors J.*, vol. 16, no. 15, pp. 6122–6129, Aug. 2016.

[4] O. Frank *et al.*, "Development of a universal stress sensor for graphene and carbon fibres," *Nature Commun.*, vol. 2, p. 255, Mar. 2011.

[5] C. Jacq, B. Lüthi, T. Maeder, O. Lambercy, R. Gassert, and P. Ryser, "Thick-film multi-DOF force/torque sensor for wrist rehabilitation," *Sens. Actuators A, Phys.*, vol. 162, no. 2, pp. 361–366, 2010.

[6] S.-H. Bae, Y. Lee, B. K. Sharma, H.-J. Lee, J.-H. Kim, and J.-H. Ahn, "Graphene-based transparent strain sensor," *Carbon*, vol. 51, pp. 236–242, Jan. 2013.

[7] J. Lee *et al.*, "Conductive fiber-based ultrasensitive textile pressure sensor for wearable electronics," *Adv. Mater.*, vol. 27, no. 15, pp. 2433–2439, 2015.

[8] J. Chen *et al.*, "Harmonic-resonator-based triboelectric nanogenerator as a sustainable power source and a self-powered active vibration sensor," *Adv. Mater.*, vol. 25, no. 42, pp. 6094–6099, 2013.

[9] D. J. Cohen, D. Mitra, K. Peterson, and M. M. Maharbiz, "A highly elastic, capacitive strain gauge based on percolating nanotube networks," *Nano Lett.*, vol. 12, no. 4, pp. 1821–1825, 2012.

[10] C. Pang *et al.*, "A flexible and highly sensitive strain-gauge sensor using reversible interlocking of nanofibres," *Nature Mater.*, vol. 11, no. 9, p. 795, 2012.

[11] G. R. Witt, "The electromechanical properties of thin films and the thin film strain gauge," *Thin Solid Films*, vol. 22, no. 2, pp. 133–156, 1974.

[12] G. I. Hay, P. S. A. Evans, D. J. Harrison, D. Southee, G. Simpson, and P. M. Harrey, "Characterization of lithographically printed resistive strain gauges," *IEEE Sensors J.*, vol. 5, no. 5, pp. 864–871, Oct. 2005.

[13] G. I. Hay, D. J. Southee, P. S. Evans, D. J. Harrison, G. Simpson, and B. J. Ramsey, "Examination of silver-graphite lithographically printed resistive strain sensors," *Sens. Actuators A, Phys.*, vol. 135, no. 2, pp. 534–546, 2007.

[14] A. Bessonov, M. Kirikova, S. Haque, I. Gartseev, and M. J. A. Bailey, "Highly reproducible printable graphite strain gauges for flexible devices," *Sens. Actuators A, Phys.*, vol. 206, pp. 75–80, Feb. 2014.

[15] D. Maddipatla *et al.*, "A novel flexographic printed strain gauge on paper platform," in *Proc. IEEE SENSORS*, Nov. 2015, pp. 1–4.

[16] B. Andò and S. Baglio, "All-inkjet printed strain sensors," *IEEE Sensors J.*, vol. 13, no. 12, pp. 4874–4879, Dec. 2013.

[17] C. S. Jones, X. Lu, M. Renn, M. Stroder, and W.-S. Shih, "Aerosol-jet-printed, high-speed, flexible thin-film transistor made using single-walled carbon nanotube solution," *Microelectron. Eng.*, vol. 87, no. 3, pp. 434–437, 2010.

[18] S. H. Ko *et al.*, "All-inkjet-printed flexible electronics fabrication on a polymer substrate by low-temperature high-resolution selective laser sintering of metal nanoparticles," *Nanotechnology*, vol. 18, no. 34, p. 345202, Aug. 2007.

[19] M. Covarrubias, A. Mansutti, M. Bordegoni, and U. Cugini, "Flexible touch sensor for evaluating geometric properties of virtual shapes through sound: This paper reports a sonification approach to visualise geometric features that are missing in haptic display," *Virtual Phys. Prototyping*, vol. 10, no. 2, pp. 77–89, 2015.

[20] V. Francis and P. K. Jain, "3D printed polymer dielectric substrates with enhanced permittivity by nanoclay inclusion," *Virtual Phys. Prototyping*, vol. 12, no. 2, pp. 107–115, 2017.

[21] H. Tan, T. Tran, and C. Chua, "A review of printed passive electronic components through fully additive manufacturing methods," *Virtual Phys. Prototyping*, vol. 11, no. 4, pp. 271–288, 2016.

[22] S. Li, J. G. Park, S. Wang, R. Liang, C. Zhang, and B. Wang, "Working mechanisms of strain sensors utilizing aligned carbon nanotube network and aerosol jet printed electrodes," *Carbon*, vol. 73, pp. 303–309, Jul. 2014.

[23] M. Hedges and A. B. Marin, "3D aerosol jet printing-adding electronics functionality to rp/rm," in *Proc. DDMC Conf.*, 2012, pp. 14–15.

[24] T. Blumenthal, V. Fratello, G. Nino, and K. Ritala, "Conformal printing of sensors on 3D and flexible surfaces using aerosol jet deposition," *Proc. SPIE*, vol. 8691, p. 86910P, Apr. 2013.

[25] D. Zhao, T. Liu, M. Zhang, R. Liang, and B. Wang, "Fabrication and characterization of aerosol-jet printed strain sensors for multifunctional composite structures," *Smart Mater. Struct.*, vol. 21, no. 11, p. 115008, 2012.

[26] B. Thompson and H.-S. Yoon, "Aerosol printed carbon nanotube strain sensor," *Proc. SPIE*, vol. 8346, p. 83461C, Mar. 2012.

[27] B. Thompson and H.-S. Yoon, "Aerosol-printed strain sensor using PEDOT:PSS," *IEEE Sensors J.*, vol. 13, no. 11, pp. 4256–4263, Nov. 2013.

[28] A. A. S. Mohammed, W. A. Moussa, and E. Lou, "High sensitivity MEMS strain sensor: Design and simulation," *Sensors*, vol. 8, no. 4, pp. 2642–2661, 2008.

[29] Y. Jia, K. Sun, F. J. Agosto, and M. T. Quinones, "Design and characterization of a passive wireless strain sensor," *Meas. Sci. Technol.*, vol. 17, no. 11, p. 2869, 2006.

[30] L. Cao, T. S. Kim, S. C. Mantell, and D. L. Polla, "Simulation and fabrication of piezoresistive membrane type MEMS strain sensors," *Sens. Actuators A, Phys.*, vol. 80, no. 3, pp. 273–279, 2000.

[31] W. Schomburg, Z. Rummler, P. Shao, K. Wulff, and L. Xie, "The design of metal strain gauges on diaphragms," *J. Micromech. Microeng.*, vol. 14, no. 7, p. 1101, 2004.

[32] J. C. Case, E. L. White, and R. K. Kramer, "Soft material characterization for robotic applications," *Soft Robot.*, vol. 2, no. 2, pp. 80–87, 2015.

[33] J. Dolbow and M. Gosz, "Effect of out-of-plane properties of a polyimide film on the stress fields in microelectronic structures," *Mech. Mater.*, vol. 23, no. 4, pp. 311–321, Aug. 1996.

[34] J. Navratil, M. Pavec, J. Reboun, T. Rericha, and A. Hamacek, "Aerosol Jet silver printed lines on subsequently bent glass substrates," in *Proc. 40th Int. Spring Seminar Electron. Technol. (ISSE)*, May 2017, pp. 1–4.

[35] S. Agarwala, G. L. Goh, and W. Y. Yeong, "Optimizing aerosol jet printing process of silver ink for printed electronics," in *Proc. IOP Conf. Mater. Sci. Eng.*, vol. 191, no. 1, 2017, p. 012027.

[36] K. Hoffmann, *An Introduction to Measurements Using Strain Gages*. Darmstadt, Germany: Hottinger Baldwin Messtechnik, 1989.

[37] W. M. Murray and W. R. Miller, *The Bonded Electrical Resistance Strain Gage: An Introduction*. London, U.K.: Oxford Univ. Press, 1992.

[38] J. Herrmann *et al.*, "Nanoparticle films as sensitive strain gauges," *Appl. Phys. Lett.*, vol. 91, no. 18, p. 183105, 2007.

[39] J. Lee *et al.*, "A stretchable strain sensor based on a metal nanoparticle thin film for human motion detection," *Nanoscale*, vol. 6, pp. 11932–11939, Aug. 2014.

SHWETA AGARWALA received the Ph.D. degree in electronics engineering from the National University of Singapore, in 2012, with a focus on nanostructured materials for dye-sensitized solar cells. She is currently a Research Fellow with SC3DP, NTU. Her research is aimed at printed electronics, 3-D printing, bioprinting and materials for electronics, and biomedical and aerospace applications.

GUO LIANG GOH received the bachelor's degree in aerospace engineering from Nanyang Technological University, Singapore, in 2015. He is currently pursuing the Ph.D. degree with the School of Mechanical and Aerospace Engineering, NTU. His current research works focus on printed flexible and stretchable electronics using additive manufacturing especially aerosol jet printing.

WAI YEE YEONG is currently an Associate Professor with the School of Mechanical and Aerospace Engineering, Nanyang Technological University. Her main research interest is in 3-D printing and bioprinting of multi-functional structures, printed electronics, and bio-electronic platforms. She has published two textbooks in 3-D printing and her h-index is 18. She is an associate editor for two international journals which are indexed in ESCI Web-of-Science database.